Environmental Science Processes & Impacts

PAPER

View Article Online
View Journal

Cite this: DOI: 10.1039/c9em00024k

Emerging investigator series: primary emissions, ozone reactivity, and byproduct emissions from building insulation materials†

Kyle Chin,[a] Aurelie Laguerre,[a] Pradeep Ramasubramanian,[a] David Pleshakov,[a] Brent Stephens[b] and Elliott T. Gall *[a]

Building insulation materials can affect indoor air by (i) releasing primary volatile organic compounds (VOCs) from building enclosure cavities to the interior space, (ii) mitigating exposure to outdoor pollutants through reactive deposition (of oxidants, *e.g.*, ozone) or filtration (of particles) in infiltration air, and (iii) generating secondary VOCs and other gas-phase byproducts resulting from oxidant reactions. This study reports primary VOC emission fluxes, ozone (O_3) reaction probabilities (γ), and O_3 reaction byproduct yields for eight common, commercially available insulation materials. Fluxes of primary VOCs from the materials, measured in a continuous flow reactor using proton transfer reaction-time of flight-mass spectrometry, ranged from 3 (polystyrene with thermal backing) to 61 (cellulose) μmol m^{-2} h^{-1} (with total VOC mass emission rates estimated to be between ~0.3 and ~3.3 mg m^{-2} h^{-1}). Major primary VOC fluxes from cellulose were tentatively identified as compounds likely associated with cellulose chemical and thermal decomposition products. Ozone-material γ ranged from $\sim 1 \times 10^{-6}$ to $\sim 30 \times 10^{-6}$. Polystyrene with thermal backing and polyisocyanurate had the lowest γ, while cellulose and fiberglass had the highest. In the presence of O_3, total observed volatile byproduct yields ranged from 0.25 (polystyrene) to 0.85 (recycled denim) moles of VOCs produced per mole of O_3 consumed, or equivalent to secondary fluxes that range from 0.71 (polystyrene) to 10 (recycled denim) μmol m^{-2} h^{-1}. Major emitted products in the presence of O_3 were generally different from primary emissions and were characterized by yields of aldehydes and acetone. This work provides new data that can be used to evaluate and eventually model the impact of "hidden" materials (*i.e.*, those present inside wall cavities) on indoor air quality. The data may also guide building enclosure material selection, especially for buildings in areas of high outdoor O_3.

Received 14th January 2019
Accepted 22nd March 2019

DOI: 10.1039/c9em00024k

rsc.li/espi

Environmental significance

Building enclosures affect indoor air through primary pollutant emissions from building materials, filtering outdoor air, and secondary emissions from reactions between oxidants (such as ozone, O_3) and materials within cavities. Infiltration of outdoor air across the building envelope is often the dominant pathway by which ambient O_3 (a primary driver of oxidation chemistry in buildings) penetrates indoors, particularly in residences. This work investigates primary VOC emissions, O_3 reaction probabilities, and O_3 reaction byproduct formation yields from eight insulation materials commonly used in building enclosures. To our knowledge, this study provides the broadest characterization of these properties for building insulation materials to date. Parameterizations reported here can enable models of outdoor-to-indoor O_3 transport and inform material selection to reduce an overlooked source (wall cavity materials) of VOCs to the indoor environment.

1 Introduction

Building envelopes impact indoor air quality in three general ways: (i) primary emissions of air pollutants from materials used in the enclosure to the interior space, (ii) incidental removal of outdoor air pollutants that cross the enclosure through reactive deposition of oxidants (such as ozone, or O_3) or filtration of particles, and (iii) secondary emissions of air pollutants resulting from reactions between infiltrating oxidants (*e.g.*, O_3) and materials used in the enclosure. Whether the impact of the building enclosure on indoor air quality is beneficial or detrimental to the exposure of occupants is dependent on a large number of factors, including (but not limited to) material selection, environmental conditions, airflow characteristics, and the quantity and type of indoor and outdoor air pollutants present.

[a]Portland State University, Mechanical and Materials Engineering, Portland, OR, USA. E-mail: gall@pdx.edu

[b]Illinois Institute of Technology, Civil, Architectural, and Environmental Engineering, Chicago, IL, USA

† Electronic supplementary information (ESI) available. See DOI: 10.1039/c9em00024k

Through emission, removal, and transformation, building enclosures impact the balance of indoor volatile organic compounds (VOCs) and O_3. Volatile organic compounds are a well-studied class of indoor air pollution, and VOCs often exceed chronic health standards indoors.[1] Ozone is a major driver of indoor chemistry and one of the most studied oxidants in indoor air.[2] Elevated concentrations of outdoor, ground-level O_3 are consistently associated with increases in a number of adverse health effects including mortality,[3–5] exacerbation of asthma symptoms,[6] and infant respiratory and cardiovascular effects.[7] In 2005, ambient O_3 was estimated to account for ~4700 deaths and ~36 000 years of life lost in the United States alone, suggesting that despite significant improvements in outdoor air quality in recent decades, levels of outdoor O_3 still pose a risk to public health.[8]

Primary emissions of VOCs from materials in building enclosure cavities contribute substantially and directly to indoor VOC concentrations.[9–11] Building enclosure materials also act as a "hidden" transformation pathway as infiltration air enters a building. For example, in the vast majority of residences in the U.S., which typically do not have mechanical ventilation systems with dedicated outdoor air supply,[12] occupants are exposed to O_3 and O_3 reaction byproducts (including VOCs) only after O_3-laden air penetrates through leaks in the building enclosure.[13–15] In U.S. residences, limited data suggests that windows are seldom open in most climates, less than 15% of the time in most cases.[16,17] Therefore, infiltration across the building envelope is often the primary path by which O_3 and O_3-building enclosure reaction byproducts enter occupied residential spaces.[18] Cracks and gaps in the building enclosure where infiltration occurs create the potential for O_3 chemistry with interior enclosure materials, such as exterior cladding, insulation, and structural materials, depending on the reactivity of the materials used and the nature of crack geometries.[15,19,20] Reactions within the building enclosure can serve to reduce the amount of outdoor O_3 that transports indoors through surface chemistry that alters the balance of O_3 and may generate harmful or irritating O_3 reaction byproducts found indoors.

To date, O_3 penetration factors have been measured in only a very limited number of buildings. In a sample of eight homes in Austin, TX, the first measurements of O_3 penetration factors (measured at an artificially high indoor/outdoor pressure difference) ranged from as low as ~0.6 to as high as ~1.0.[21] Subsequent measurements of O_3 penetration factors in a multi-family apartment unit during natural infiltration conditions revealed a mean value of only 0.54.[22] These data suggest that most homes relying on infiltration for ventilation air likely have O_3 penetration factors lower than unity (*i.e.*, $P_{O_3} \leq 1$). In homes under these conditions, as much as 40–50% of total outdoor O_3 loss occurred because of reactions within the building enclosure, offering substantial protection from indoor ozone exposure, but with implications for subsequent exposure to byproducts of O_3 reactions within the building enclosure that may be transported indoors.

If O_3 reactions occur primarily at the enclosure, indoor exposures to infiltrated O_3 are likely lower than if reaction losses occur primarily with indoor materials and reactive gas-phase compounds. Indoor exposure to O_3 reaction byproducts formed from homogeneous or heterogeneous indoor O_3 chemistry are also likely to be different, due to the distinct materials that are present in building enclosures *versus* in interior occupied spaces. Some known byproducts of indoor O_3 reactions with common surfaces and/or gases in typical indoor environments include organic acids, carbonyls, free radicals, and secondary organic aerosols,[23–26] all of which can yield varied inflammatory responses in humans. Understanding routes of indoor O_3 removal and transformation are warranted given that O_3 oxidation products may be partially responsible for the health impacts of ambient O_3 observed in epidemiology studies.[16]

Ozone reaction probabilities of typical building enclosure materials available in the literature range several orders of magnitude, from $\sim 10^{-4}$ for brick to $\sim 10^{-8}$ for aluminum.[15] Key material properties that influence O_3 reaction probability are porosity, thickness, and composition.[27] However, there exists very limited data in the literature reporting O_3 reaction probabilities to materials used inside building enclosures (*e.g.*, various insulation types, soundproofing, *etc.*) and little data reporting the emissions of volatile byproducts stemming from these materials in the presence or absence of O_3. Therefore, this study evaluates primary VOC emissions, O_3 reaction probabilities, and O_3 reaction byproduct yields for eight common, commercially available building insulation materials to further understanding of how insulation selection in building enclosures may affect indoor air through these mechanisms.

2 Methods

2.1 Test materials

Eight commercially available insulation materials that are commonly used in building enclosures were selected to span a wide range of chemical composition and physical properties: fiberglass, cellulose, stone wool, recycled denim, polystyrene, polyurethane spray foam, polystyrene with a thermal backing, and polyisocyanurate foam. An overview of properties of the test materials is provided in Table 1. Images of each tested material in its raw form and as prepared for testing are provided in the Table S1 in the ESI.†

All tested materials were purchased new. A sub-sample of each material was randomly taken from the larger quantity of each purchased product. Samples were made to accommodate placement in a benchtop scale environmental chamber (see Section 2.2) for measurement of VOC emissions, O_3 dry deposition, and reaction byproducts emitted after being exposed to O_3. Materials were of varying morphology and bulk structure and were prepared to ensure a known, projected surface area was exposed to the bulk chamber air. Materials made of loose fill (cellulose, fiberglass, stone wool, denim) were placed in a glass enclosure (Pyrex) with taped edges. Solid materials were cut with the sides and backing sealed with aluminium tape to expose only the top surface to the chamber environment.

Table 1 Summary of characteristics of tested building enclosure materials

Manufacturer	Name/material[a]	Code	Sample mass (g)	Exposed area (cm^2)	v_t used[b]
Owens Corning	Fiberglass	FG	11.8	74.6	FG
GreenFiber	Cellulose	C	54.9	74.6	C
Touch 'n foam	Polyurethane	PU	31.3	88.1	PI
Thermasheath	Polyisocyanurate	PI	24.9	148.5	PI
Roxul	Stone wool	SW	24.9	74.6	FG
R-Tech	Polystyrene w/thermal backing	PSTB	11.8	136.2	PS
Cellofoam	Polystyrene	PS	8.1	145.9	PS
UltraTouch	Recycled denim	DM	25.3	74.6	FG

[a] An image of each material in its raw form and as prepared for testing is available in the ESI. [b] FG = fiberglass, C = cellulose, PI = polyisocyanurate, PS = polystyrene.

2.2 Chamber apparatus and instrumentation

Samples were tested for source and sink behaviour in a 11.4 L laboratory chamber apparatus; detailed descriptions of a similar experimental apparatus are available in Gall and Rim.[28] Briefly, the experimental apparatus was an electropolished stainless steel chamber (CTH-24, Eagle Stainless) in which flowrate, temperature, and humidity conditions were controlled to maintain environmental conditions. Air was supplied by laboratory compressed air supply and passed through a particle filter and granular activated carbon filter to remove particles and volatile organics in inlet air. Air was humidified to a setpoint by control of two flows, one passed through an impinging column filled with purified water and a second bypass flow. Ozone was injected into dry air (bypass flow) using a stable O_3 generator (97-0067-01, UVP). Chamber temperature was controlled by circulating the outflow of a temperature-controlled water bath (Neslab RTE 10, Thermo Scientific) through vinyl tubing wrapped around the exterior surfaces of the chamber.

All flows were controlled and measured using mass flow controllers (GFC17A, Aalborg). Inlet and chamber temperature and relative humidity were measured *via* sensors (S-THB-M-002, Onset) inserted into the chamber inlet line and through a septum in a chamber access port, respectively; the sensor which protruded slightly into the chamber was included as part of the chamber background. Ozone was monitored using a UV absorbance federal equivalent method instrument (106-L, 2BTech). The chamber was operated at a flowrate of 1.88 L min^{-1}, and target conditions of inlet O_3, temperature, and relative humidity of 100 ppb, 22 °C, and 50% RH. Actual chamber conditions were (mean across all experiments ± 1 s.d.) 100.2 ± 5.2 ppb, 21.95 ± 0.91 °C and 50.9 ± 0.51% respectively. An inlet O_3 concentration of 100 ppb was chosen to represent a high, albeit realistic, outdoor O_3 concentration that exterior building enclosures are subjected to in a high ambient O_3 environment.

2.3 Volatile organic compound measurements

Primary emissions of volatile organic compounds (VOCs, primary emissions calculated in the absence of O_3) and byproduct formation yields (VOCs emitted due to O_3 surface flux) were calculated with established methods (Lamble *et al.*[29]) using concentration data measured *via* proton transfer reaction-time of flight-mass spectrometry (PTR-TOF1000, Ionicon). The PTR-TOF-MS scanned across 17–250 amu for compounds with a proton affinity higher than that of H_2O. The drift tube conditions were 600 V, 60 °C, and 2.28 mbar. The PTR-TOF-MS was operated at an E/*N* value of 130. The mass axis was calibrated to three peaks: NO (m/z = 29.9974), $C_3H_7O^+$ (m/z = 59.0497) and a $C_6H_4I_2$ fragment (m/z = 203.944) that was continuously injected into the drift tube *via* a heated permeation device (PerMaScal, Ionicon). The PTR-TOF-MS inlet was maintained at 60 °C and the supplemental inlet flow to the drift tube was 50 mL min^{-1}. Mass spectra were stored in 10 s intervals.

Compounds were first identified using a peak table resolved with unit mass resolution. This method was selected given the limitations associated with the mass resolving power of the PTR-TOF1000 ($m/\Delta m \sim 1000$). Ions known to be associated with instrument operation were removed from the analysis (m/z 29, 30, 32, 34, 36, 37, 38, 39, 46, 50).[30] Compounds meeting a threshold of statistically significant difference due to the material or material and O_3 presence (Section 2.5.3) are first identified according to their unit mass. For observed primary fluxes and yields, the five largest contributors to flux or yield are assigned an exact mass from the measured mass, determined from the centroid of the peak of interest by manual inspection of mass spectra (PTR-MS Viewer 3.2.12, Ionicon). The five largest contributors to flux are discussed in terms of their putative chemical identification (ID), determined from evaluation of potential chemical formulas that may result in the exact mass of each signal, analysis for presence of expected isotopes for a given chemical ID, and a review of the literature for compounds expected to be emitted from test materials in the presence or absence of O_3.

Following assignment of the five largest fluxes or yields, the remaining mass was allocated into groups based on unit mass by carbon and hydrogen containing compounds (C_xH_y) and oxygenated compounds containing one (C_xH_yO) and two oxygen atoms ($C_xH_yO_2$). The approach was similar to that of Inomata *et al.*;[31] compounds were classified by attribution of a general chemical formula based on the known series of families of

compounds across a range of one to fifteen carbon atoms. Dienes (m/z 55 + 14n), aromatics (m/z 79 + 14n), and alkenes (m/z 43 + 14n) were assigned to C_xH_y. The series m/z 43 + 14n may also represent unsaturated aldehydes; only m/z 43, 57, 71, and 85 were assigned from this series based on manual inspection of spectra for each compound at these m/z for each material tested. Assignment to C_xH_y or C_xH_yO was based on the closest alignment of the exact mass and expected isotopes due to presence or absence of oxygen. Saturated aldehydes and ketones (m/z 31 + 14n), phenols (m/z 95 + 14n), and m/z 33 were assigned to C_xH_yO. Along the series m/z 47 + 14n, mono- and di-oxygenated compounds were distinguished by manual inspection of mass spectra for expected isotopes from compounds containing two *vs.* one oxygen atoms and assigned to either C_xH_yO or to $C_xH_yO_2$. All other compounds remained unidentified as "other" mass flux.

Volatile organic compounds were quantified with the PTR-TOF-MS using a relative transmission method similar to methods described elsewhere.[32] A transmission curve was generated using eight calibration compounds spanning protonated mass of 33 to 135 (methanol, 1,3-butadiene, methyl vinyl ketone, benzene, toluene, *p*-xylene, 1,3,5-trimethyl benzene, 1,2,3,5-tetramethyl benzene). Calibration compounds were diluted to 100 ppb from an initial nominal mixing ratio of 2 ppm from a compressed gas cylinder (Airgas) using a dilution system that mixed a known flowrate of zero air (Airgas) with a known flowrate from the compressed cylinder containing gas standards. The relative transmission method requires an estimate of the mixing ratio of H_3O^+ isotope, typically approximated from the mass signal of the isotope at m/z 21.022. We determined this parameter using the generated transmission curve from the data analysis software for the instrument (PTR-MS Viewer 3.2.12, Ionicon) and calculating a best-fit value of transmission at m/z 21.022 that resulted in the minimization of the sum of squared errors between the reported concentration of the eight compounds used in generation of transmission curve and the known concentrations from the diluted calibration standard. Using this method, reported concentrations for all compounds in the calibration curve were estimated with the transmission method to within 20% of calibration value. For compounds present in the calibration standard, reaction rate constants were taken from Zhao and Zhang.[33] For other compounds, quantification was made using the transmission factor and the Ionicon default reaction rate constant of 2×10^{-9} cm^3 per s per molecule. After calculation *via* the transmission curve, quantification of the five largest primary emission fluxes or yields was corrected for isotopologues by correcting the major signal for its contribution to the total mass of the compound.[34] Reported concentrations for the five largest primary emissions sources or sinks and yields are corrected by manual inspection of peak assignment, correction for known isotopic interferences when greater than 1%, and deconvolution of overlapping peaks where instrument resolution is sufficient (*e.g.*, separation of protonated methanol (m/z 33.0335) from one oxygen-17 isotopologue of O_2^+ (m/z 32.9971)). These analyses were all performed in PTR-MS Viewer 3.2.12 (Ionicon).

2.4 Experimental protocol

Prior to initiation of experiments, the stainless-steel chamber surfaces and test material glass enclosures were cleaned and passivated to reduce background reactions between O_3 and chamber surfaces. The chamber and enclosures were first cleaned with water and soap and rinsed three times. Surfaces were rinsed with reagent grade isopropyl alcohol followed by methanol, followed by hexane (all compounds Sigma-Aldrich, 98% or greater purity). Surfaces were allowed to dry in a fume hood overnight and were then heated with a heat gun. The day before an experiment, the chamber was passivated by introducing elevated O_3 (>500 ppb) into the chamber for at least 10 hours.

The experimental protocol included measurement of VOCs and O_3 levels in the inflow and outflow of an empty chamber (background) before and after experiments where materials were tested in the presence or absence of O_3. Volatile organic compounds and O_3 levels were measured at the chamber outlet or inlet following the timeline described in Fig. 1. The duration of each sample period was selected by calculation of the predicted time to reach steady-state in a non-reactive chamber. It was calculated that an unreactive chamber would reach 99% of steady-state O_3 levels after ~30 minutes; surface reactions will reduce this time to reach steady-state. The steady-state condition was confirmed for each experiment by evaluating if chamber O_3 levels deviated more than 2 ppb in the final 20 minutes of each chamber monitoring period, a similar criteria to prior studies.[35] All experiments met the steady-state criteria for chamber O_3 levels. Following the completion of each experiment, the chamber was prepared for the next experiment by passivating the chamber overnight.

2.5 Data analysis

2.5.1 Quantification of volatile organic compound source and sink strength. Primary emissions of VOCs are those compounds emitted due to the presence of the material itself, and in the context of this study, in the absence of O_3. Primary emissions from the test samples were calculated according to eqn (1):

$$E_{\text{primary}} = \frac{\lambda V(C_{\text{i,outlet}} - C_{\text{i,inlet}}) - \lambda V(C_{\text{i,outlet,BG}} - C_{\text{i,inlet,BG}})\left(1 - \frac{A_e}{A_{BG}}\right)}{A_e} \quad (1)$$

where λ is the air exchange rate (s^{-1}), V is the volume of the stainless steel chamber (cm^3), $C_{\text{i,outlet}}$ and $C_{\text{i,inlet}}$ are the concentrations of compound i in outlet and inlet chamber air with a test material present, respectively (ppb), $C_{\text{i,outlet,BG}}$ and $C_{\text{i,inlet,BG}}$ are the concentrations of compound i in outlet and inlet chamber air for an empty chamber test, respectively (ppb) and A_e and A_{BG} are the surface areas of the exposed sample and the stainless steel chamber, respectively (cm^2).

The molar yield describes the amount of byproduct formed as a result of chemical reactions between a reactant, in this case O_3, and the material, normalized by the flux of O_3 to the

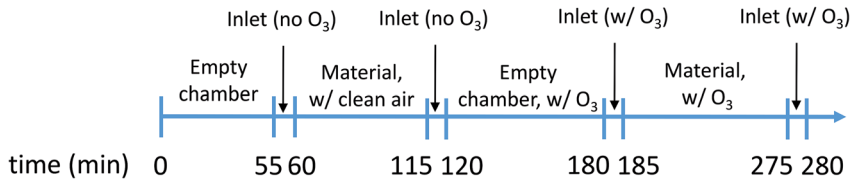

Fig. 1 Summary of experimental protocol for testing of ozone reaction probabilities, primary emissions of volatile organic compounds and byproduct formation yields.

surface.[36] The molar yield was calculated following the method described by Lamble *et al.*,[29] shown in eqn (2):

$$Y_i = \frac{C_{i,outlet,O_3} - C_{i,outlet,o}}{C_{O_3,in} - C_{O_3,e}} \quad (2)$$

where Y_i is the molar yield of compound i (moles i formed per moles O_3 consumed, or mol mol^{-1}), $C_{i,outlet,O_3}$ is the concentration of compound i following O_3 exposure, $C_{i,outlet,o}$ is the concentration of compound i prior to O_3 exposure, $C_{O_3,in}$ is the concentration of O_3 at the chamber inlet, and $C_{O_3,e}$ is the concentration of O_3 at the chamber outlet (ppb), corrected for losses to chamber walls.

2.5.2 Ozone deposition. The deposition velocity (v_d) of a test material was calculated from measurement of inlet and outlet O_3 levels from experiments conducted with an empty chamber and the chamber containing a test material sample. The steady-state O_3 deposition velocity is calculated as described previously[37] and shown in eqn (3):

$$v_d = \lambda \frac{V}{A_e}\left(\frac{C_{inlet}}{C_{outlet}} - 1\right) - v_{d,BG}\frac{A_{BG}}{A_e} \quad (3)$$

where C_{inlet} and C_{outlet} represent the O_3 concentrations in the inlet and outlet air flow of the chamber, respectively (ppb), and v_d and $v_{d,BG}$ are the O_3 deposition velocities for test material and chamber, respectively (cm s^{-1}) and all other terms as described previously.

Background O_3 deposition velocities ($v_{d,BG}$) are calculated by performing an experiment with an empty chamber for a fixed air exchange rate until steady-state O_3 concentrations are achieved. Inlet and outlet concentrations of O_3 averaged over the final 20 minutes of data collection are used to solve eqn (3) for $v_{d,BG}$ when $v_d = 0$ and there is no exposed test material area (A_e). To measure the deposition velocity to the insulation material (v_d), the test procedure is repeated for experiments with insulation materials placed in the chamber, and eqn (3) is solved for the unknown values of v_d. An estimate of uncertainty was calculated using a propagation of errors, incorporating uncertainties of the O_3 monitors of 2% of reading and flow controllers of 1.5%.

Ozone deposition was further parameterized by determining the material reaction probability (γ, dimensionless), or the fraction of O_3 molecule-surface collisions that result in a reaction. To calculate the reaction probability, the transport limited deposition velocity (v_t, cm s^{-1}) was first determined by applying potassium iodide to surfaces using previously described protocols[27] and γ was calculated using eqn (4) as described by Cano-Ruiz *et al.* (1993):[38]

$$\gamma = \frac{4}{\langle v_b \rangle}\left(\frac{1}{v_d} - \frac{1}{v_t}\right)^{-1} \quad (4)$$

where $\langle v_b \rangle$ is the Boltzmann velocity, and is equal to 3.6110 cm s^{-1} for O_3 at 22 °C.

As shown in Table 1, we determined the transport-limited deposition velocity experimentally for four different materials. For materials for which v_t was not directly calculated, we assigned a v_t value for the material with the most similar surface morphology (see Table 1), similar to the approach taken by Lamble *et al.*[29] Uncertainty in reaction probabilities was calculated from a propagation of errors from experiments conducted to determine $v_{d,BG}$, v_d, and v_t.

2.5.3 Statistical testing for significant VOC emissions. Data generated by the PTR-TOF-MS, when initially analysed with unit mass resolution, resulted in time-series mass spectra with >200 peaks each. These spectra required subsequent analysis for identification of peaks with significant differences due to material presence (primary emissions) or material and O_3 presence (molar yield). For statistical testing to identify primary emissions, we selected 100 steady-state time series data points from each of the test conditions of empty chamber outlet and chamber with material outlet. Statistical significance was determined by comparing datasets for each mass unit with a *t*-test with $\alpha = 0.05$.

For molar yields, comparisons required three groups: the empty chamber in the presence of O_3, the chamber with only the material present, and the chamber with the material and O_3 present. As with statistical testing for primary emissions, 100 steady-state time series data points were selected for each of the three test conditions. Statistical testing required consideration of multiple comparisons; thus, 3-group ANOVA was used to determine if statistically significant differences existed across comparisons. The ANOVA *F*-test was first calculated for each mass signal to determine if at least two of the means across groups were significantly different. This test was performed with $\alpha = 0.05$. If the *F*-test determined at least two comparisons within the three groups were different, a *post hoc* Bonferroni-corrected *t*-test was performed for each of the three possible combinations of *t*-tests between the groups. The Bonferroni correction resulted in a *p*-value for the *t*-test statistic of 0.017. Yields were included as statistically significant only if three conditions were met: (1) the *F*-test met the significance threshold, (2) *t*-test comparison between chamber with material and O_3 and empty chamber with O_3 met *t*-test threshold, and (3) *t*-test comparison between chamber with

material and O_3 and chamber with only material present met *t*-test threshold.

3 Results and discussion

3.1 Primary emissions from building insulation materials

An example of the resulting estimation of molar fluxes across unit mass resolved mass spectra from the PTR-TOF-MS is shown in Fig. 2 for cellulose and fiberglass. Note that these emissions were those determined from the presence of the material alone, *i.e.*, in the absence of O_3. From Fig. 3, it can be observed that cellulose emits a larger quantity and more diverse range of volatile organic compounds due to the material itself compared to fiberglass, expected given the organic nature of cellulosic material *vs.* the higher inorganic content present in the fiberglass material. Mass to charge ratios where no flux is reported are those *m*/*z* ratios where the comparison of the empty chamber to the chamber with material did not meet the statistical threshold for significance ($\alpha > 0.05$).

A summary of primary emission source and sink behaviour is shown in Fig. 3 for all tested materials. Detailed tables showing mass accuracy, putative chemical ID, and additional notes can be found in the ESI in Table S2.† In general, the tested materials acted as a source of VOCs to the chamber outlet, although in some circumstances statistically significant decreases in chamber levels for specific VOCs compared to background tests were detectable for some materials. Note that for each statistically significant mass signal (see Section 2.5.3) from the PTR-TOF-MS, the compound was considered as a source if eqn (1) was positive for that mass signal and a sink if eqn (1) was negative. Thus, as shown in Fig. 3, materials exhibit may act as a source for certain compounds while acting as a sink for others.

Cellulose insulation was the largest emitter of VOCs followed by recycled denim. Interestingly, both materials are made from recycled materials, as the cellulose was primarily derived from recycled newsprint. Cellulose is also one of the major components of denim,[39] explaining the similar magnitude and composition of observed primary VOC fluxes. PSTB, when subtracting positive VOC fluxes (sources) from negative VOC fluxes (sinks), had the lowest VOC emissions of all tested materials, due in part to the modest sink effect observed for compounds *m*/*z* 47.0131, *m*/*z* 45.031, and *m*/*z* 61.0289 (see Table S2†).

A thorough exploration of the potential chemical mechanisms impacting primary emissions for each material is beyond the scope of this paper but may be warranted in the future given the relatively high primary emissions observed here for some materials. In the case of cellulose, the largest emitter, there exists a body of research demonstrating the instability of cellulose and release of VOCs. As noted previously, cellulose is also a common recycled insulation material, and is present in many other consumer products present indoors. For the five largest significant fluxes from cellulose, we speculate that chemical assignments are protonated methanol (CH_3OH), an acid fragment possibly associated with isopropyl alcohol,[40] acetaldehyde (C_2H_4O), formic acid (CH_2O_2) and acetic acid (CH_3COOH). Note that because of the limitations with the mass resolving power of the instrument and resulting potential for interferences, these assignments should be taken as tentative chemical identifications.

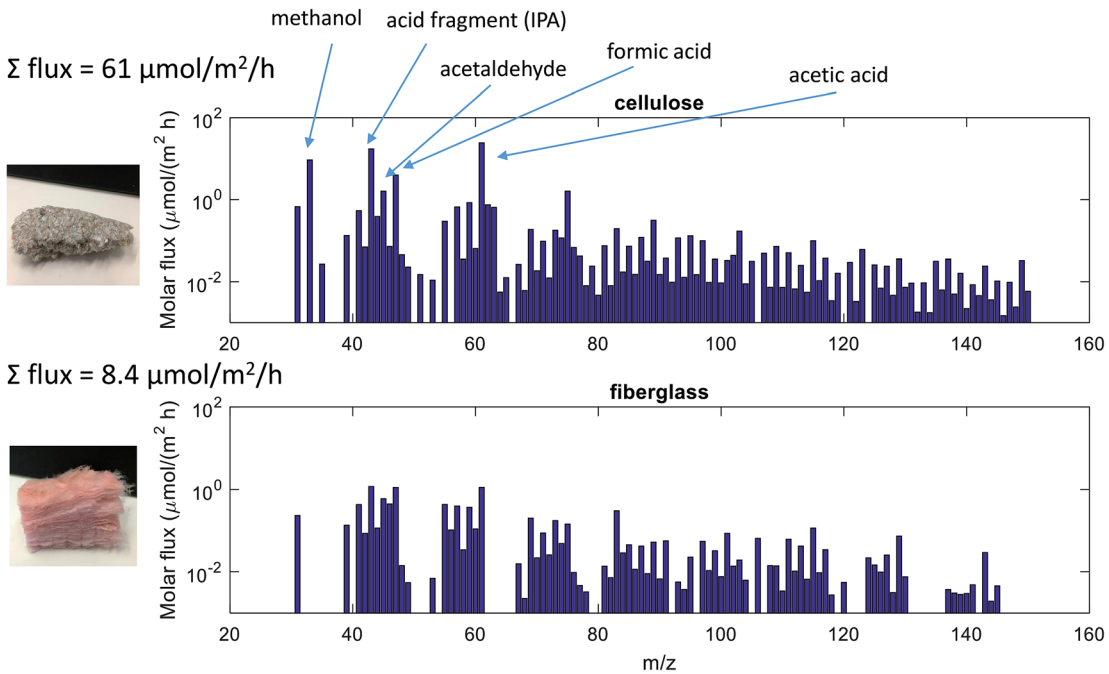

Fig. 2 Example of unit mass resolution spectra for calculation of primary emission fluxes from cellulose and fiberglass across *m*/*z* 20–160. Putative chemical identification is shown for cellulose based on further analysis of exact mass, isotopic ratio, and survey of the literature for likely compounds emitted from the material.

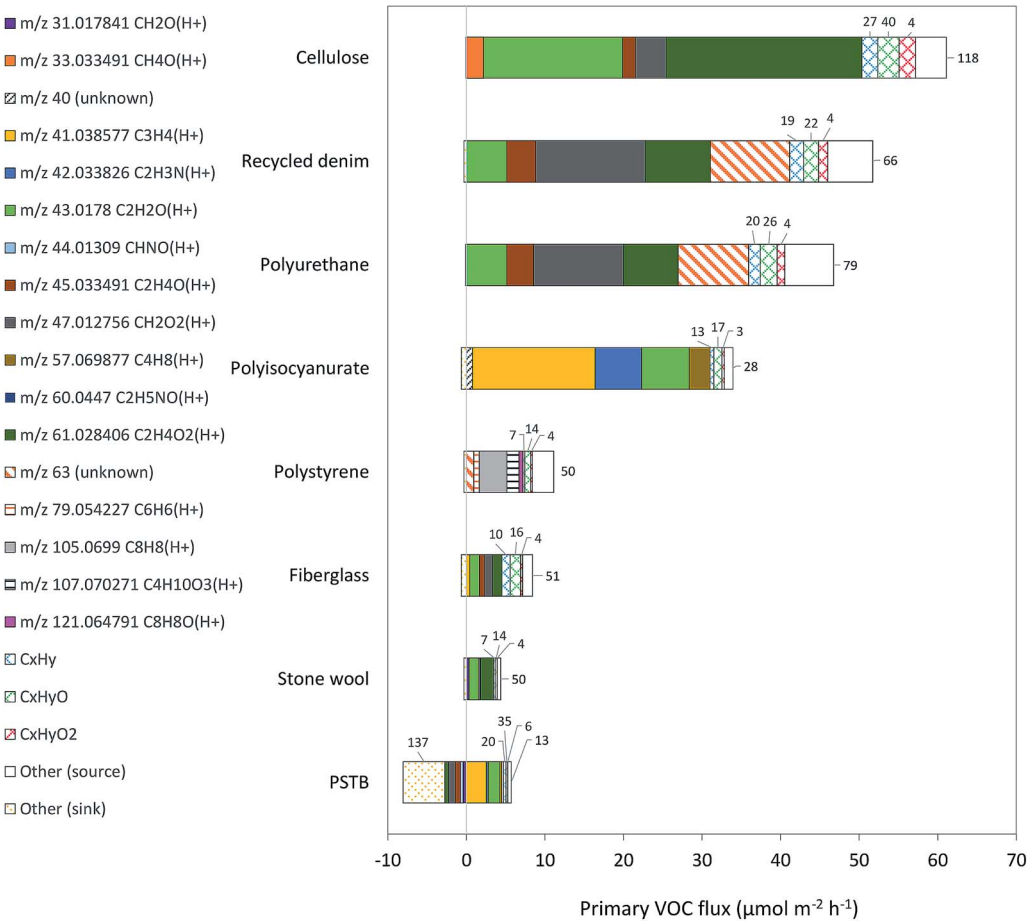

Fig. 3 Summary of primary emissions of volatile organic compound sources and sinks for each material. Note that the data labels on the C_xH_y, C_xH_yO, $C_xH_yO_2$, and other categories refer to the number of unique, statistically significantly elevated compounds identified in the comparison of the empty chamber to the chamber with a material present. These compounds were identified with unit mass resolution. PSTB = polystyrene with thermal backing.

Cellulose is known to be a reactive material, subject to a wide variety of degradation routes including chemical, thermal, and radiation induced reaction routes;[41] the largest primary emissions from cellulose may be explained from a variety of cellulose degradation mechanisms. Low molecular weight organic acids are known to be formed from degradation of polysaccharide chains in cellulose materials, forming acetic acid and formic acid.[42] Acetic acid was the highest measured flux (24.2 µmol m^{-2} h^{-1}) from cellulose insulation, and has been observed as an emitted product from degradation of cellulose-containing museum materials.[43] Methanol and acetic acid have also been observed in FLEC cell studies of emissions from various solid wood products.[44] Note that wood is typically on the order of 40–50% cellulose.[45] Acetaldehyde is a commonly identified indoor air pollutant;[1] the presence of acetaldehyde flux from cellulose insulation may derive from aerobic microbial activity, possibly from the oxidation of ethanol present as a solvent in adhesives.[46] The presence of ethanol in the material is plausible as the cellulose insulation is made from recycled newsprint; inks contain a variety of solvents including ethanol.[47] We attribute the peak at *m*/*z* 47 to formic acid and not ethanol due to its alignment with the exact mass of formic acid (*m*/*z* 47.0128) and the presence of isotopes of intensity and at exact masses (*m*/*z* 48.01611 and *m*/*z* 49.017) expected for formic acid in the mass spectra. However, it is possible that volatile ethanol is present in our air sample at relatively low mixing ratio but is not distinguishable from the formic acid peak. Furfural is a known marker of cellulose degradation,[48] and has been detected previously with PTR-TOF-MS at *m*/*z* 97.0287 (protonated parent compound) and *m*/*z* 62.0334 (fragment).[49] Both signals are statistically significantly elevated in the cellulose mass spectra, and in combination total a flux of ~1.1 µmol m^{-2} h^{-1} of furfural; or the 7th largest observed VOC flux.

Interestingly, polyurethane primary VOC emissions appeared similar to that of cellulose containing materials (cellulose and recycled denim). Some polyurethane spray foams may include cellulosic materials,[50] although the material safety data sheet (MSDS) for the polyurethane spray foam material used here did not list cellulose as part of the composition. There is limited data in the peer-reviewed literature on VOC emissions from polyurethane spray foam; a NIST report using microchambers on four spray foams reported the largest chemicals

identified as 1,4-dioxane, 1,2-dichloropropane, 1,4-dimethyl piperazine; tris-(1-chloro-2-propyl)phosphate (TCPP) and 1,2-dichlorobenzene.[51] These compounds appear not to have been the largest five emitters in our sample, however, a statistically significantly elevated signal was observed at the corresponding m/z ratios for 1,4-dioxane (exact mass = m/z 89.059706, measured mass = 89.05157). At a flux of 0.15 μmol m^{-2} h^{-1}, 1,4-dioxane would be the 19th largest VOC flux from this material. Other compounds were out of range of the PTR-TOF-MS mass range (TCPP), not detected (1,4-dimethylpiperazine and 1,2-dichloropropane), or possibly detected at very low fluxes (1,2-dichlorobenzene). However, three of the four spray foams tested in the NIST study were sampled 5–24 months after spraying. In this work, we tested the spray foam within 48 hours of spraying. Thus, we speculate that the major contributor to the observed VOCs is a result of the blowing agents used (or B-side components of this do-it-yourself spray foam kit), which may contain, *e.g.*, formic acid.[52] A NIST report notes that "a wide range of aldehydes" were detected in spray foam samples from a test house, however, the house was aged for 1.5 years and these compounds may have originated from other sources, adsorbed to the spray foam, and subsequently desorbed during sampling.[53]

Polyisocyanurate was characterized by substantial VOC emissions from m/z 41.038577 and m/z 42.033826. We speculate that m/z 41.038577 is protonated propyne (C_3H_4), likely a fragment of a larger molecule based on prior studies in the literature.[54,55] The signal at m/z 42 may also be associated with acetonitrile in PTR-MS studies;[56] the exact mass of acetonitrile aligned well with the measured mass and acetonitrile is a solvent which may be used in the production of polyisocyanate polymers.[57] However, it is also possible that this signal represents the fragment of propanal.[58] Other materials (polystyrene, fiberglass, stone wool, PSTB) had generally lower primary VOC emissions. Polystyrene was the only material with a large peak at m/z 105.0699, which we attribute to styrene.

On a mass basis, total primary VOC emissions summed for all statistically significant unit masses yields a total VOC (TVOC) mass flux ranging from ~0.3 mg m^{-2} h^{-1} (from PSTB) to ~3.3 mg m^{-2} h^{-1} (from cellulose). These estimates are based on the summation of statistically significantly elevated molar fluxes, assuming that the molecular weight of each compound is one amu less than the protonated mass. The complete list of statistically significant positive molar and estimated mass fluxes for cellulose and PSTB is available in Table S3.† These estimates of summed TVOC emissions are within the range of TVOC emissions reported for many polymeric building materials; for example, TVOC emissions from plywood have been shown to range 0.04–1.5 mg m^{-2} h^{-1}.[59,60] To explore the potential implications of these primary TVOC fluxes, consider a well-mixed 150 m^2 single-story home with 3 m height walls and dimensions of 10 m × 15 m. The total wall enclosure assembly area would be ~150 m^2. If windows contribute 20% of the wall enclosure area, the total wall area would be ~120 m^2. Assuming ~90% of the wall cavity is filled with the tested insulation materials (10% accounting for studs and other construction elements), and that approximately half of the wall assembly contributes VOC fluxes directly to the interior of the space (*e.g.*, if stack-driven flow dominates and leakage areas are evenly distributed along the vertical height, half would be a reasonable approximation[61]), the TVOC flux from the wall cavity could contribute between ~16 mg h^{-1} and ~180 mg h^{-1}, depending on material (and assuming mass transfer characteristics are consistent between the cavity and the chamber test conditions; a useful but somewhat unrealistic approximation). If the air exchange rate in the space is 0.5 h^{-1}, the resulting TVOC concentration would be between ~70 μg m^{-3} and ~800 μg m^{-3}. These approximations are reasonably consistent with limited prior estimates of the contribution of wall cavity materials to indoor spaces of which we are aware.[9,11] However, future work beyond the scope defined herein should integrate these findings into more mechanistic models of emissions and transport from enclosures to interior spaces.

3.2 Ozone removal to materials

Results of the calculation of deposition velocity and reaction probability are presented in Fig. 4. Ozone deposition tests were conducted in duplicate; error bars shown in Fig. 4 are the larger of propagated uncertainty or the range across duplicate tests. Results show that γ varied by more than an order of magnitude across materials, from ~1×10^{-6} to ~3×10^{-5}. These values are in the range that Liu and Nazaroff[15] predict could yield highly varying O_3 penetration factors through insulation materials alone under realistic pressure differences, ranging from ~70% penetration to <10% penetration.

There exist relatively few measurements of O_3 reactivity of building enclosure insulation materials in the literature. To the best of our knowledge, reaction probabilities have been reported only for fiberglass materials, which is discussed subsequently. Given the recent acknowledgement that building envelopes can act as a protective barrier for O_3,[21,62,63] we expect these data to be useful for modelling indoor–outdoor O_3 transport and as an aid in building enclosure material selection. In general, fibrous and loose materials (cellulose, fiberglass, stone wool and recycled denim) appeared to have generally higher γ while rigid, smoother materials (polyurethane, polystyrene, polyisocyanurate, and polystyrene with thermal backing (PSTB)) appeared to have lower γ. Given that estimates reported here are "effective" reaction probabilities, meaning they are derived from a deposition velocity parameterized to horizontal projections of test material surface area, these values are over-predictions relative to estimates that consider the internal surface area of a material.[64] As will be discussed, this consideration is of particular importance given the potential for complex and varied flow paths across or through materials in building enclosure assemblies.

We measured the transport-limited deposition velocity for four materials, selecting materials that varied in structure and morphology. Measured v_t are reported in Table S4† of the ESI,† and ranged from 0.14–0.27 cm s^{-1}, indicating potential for transport of O_3 to the surface to impact overall ozone removal for some tested materials. For the chamber conditions used, resistance due to transport and surface reaction were on the

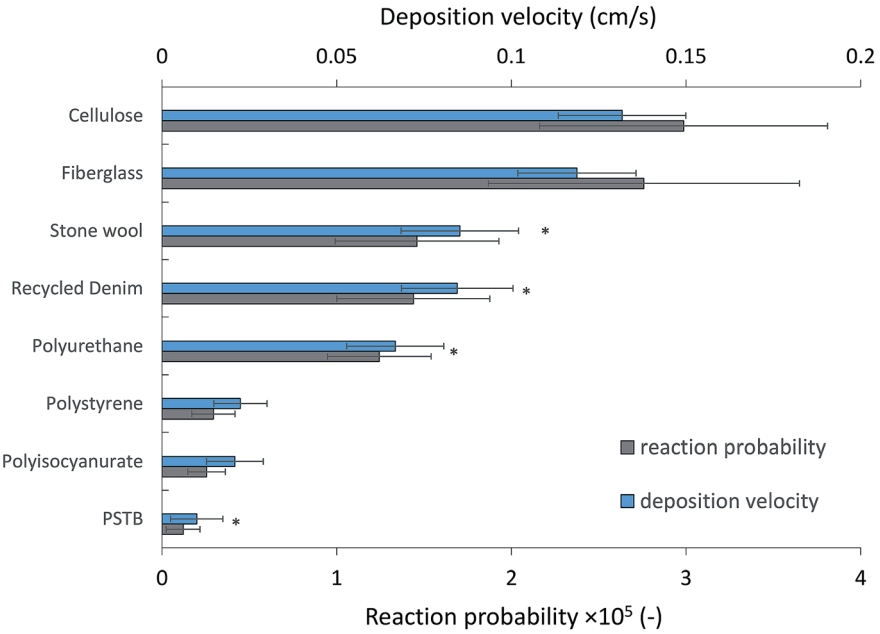

Fig. 4 Summary of ozone deposition velocities and reaction probabilities calculated for each of the eight test materials. PSTB = polystyrene with thermal backing. *Note that γ for these materials were calculated using v_t measured for another tested material with similar surface morphology. The assumed v_t results in an additional source of uncertainty in the calculation of γ for these materials, described in greater detail in the ESI in Table S4.†

same order of magnitude for five of eight tested materials (PU, DM, SW, C, FG) while for three tested materials (PI, PSTB, PS) the surface resistance dominated. Implications for uncertainty in calculated reaction probabilities are discussed the ESI.†

As described in Sections 2.1 and 2.2, materials were tested in a well-mixed continuous flow reactor (CFR) with one surface of the material prepared to allow interaction with the bulk chamber air. The parameterization of the deposition velocity requires a surface area for calculation, normally taken to be the horizontal projection of surface area. Air transport across or through materials within building enclosures is complex, but it is expected that the majority of transport occurs through pressure-driven flow across larger (0.2–1 mm in crack height) size cracks and gaps in the enclosure.[15] Liu and Nazaroff[15] discuss the likely flow paths of air entering a building enclosure filled with fiberglass insulation and conclude the airflows are likely to either traverse through a fiberglass mat in the direction orthogonal to a vertical wall or bypass insulation in the air space between the insulation and the frame. In the former case, it is likely that a fibrous mat acts as filter, with greater internal surface area available for interaction than in the latter case of airflow predominantly passing through void space.

Reaction probabilities calculated here are more likely to be representative of a scenario where air movement occurs in the void space adjacent to a material in a two-phase material–air system. While limited data exists reporting O_3 reaction probabilities to building insulation materials, Liu and Nazaroff[15] empirically estimate the reaction probability of fiberglass fibers to be 6×10^{-6}, lower than the value of 2.8×10^{-5} reported here. Note that the comparison of these reaction probabilities is for that of a fiber of fiberglass compared to the effective reaction probability made using a horizontally projected area of a material sample. In contrast, the reaction probability reported here is similar to the value of $\sim 3 \times 10^{-5}$ reported by Lamble *et al.*[29] for fiberglass ceiling tiles tested in a similar manner to the apparatus used in the present study. Liu and Nazaroff[15] use a plug flow reactor, described in detail by Morrison and Nazaroff,[65] that exposes a greater internal surface area of the material to O_3-laden flow than the continuous flow reactor (CFR) type apparatus used here and in Lamble *et al.*[29] Future studies of pollutant transport and transformation occurring in building enclosures should carefully consider the formulation, and assumptions inherent to, surface and transport resistance terms, as flow paths in building enclosures are likely complex and both spatially and temporally variant.

3.3 Ozone byproduct yields from building insulation materials

Major contributors to the O_3 byproduct yield with the tested materials appear to be oxygenated VOCs, primarily aldehydes; O_3 byproduct yields are shown in Fig. 5. Yields ranged from 0.25 (polystyrene) to 0.85 (recycled denim) moles of byproduct formed per mole of O_3 consumed (mol mol^{-1}). For the experiments conducted here, these yields are equivalent to secondary fluxes that range from 0.71 (polystyrene) to 10 (recycled denim) μmol m^{-2} h^{-1}. While lower in magnitude than the primary emissions discussed in the scaling analysis in Section 3.1, it is plausible that secondary products from O_3 reactions on wall cavity materials could impact indoor air quality. We believe these findings compel further study of the oxidation pathways in wall cavities, including coupling of outdoor–enclosure–

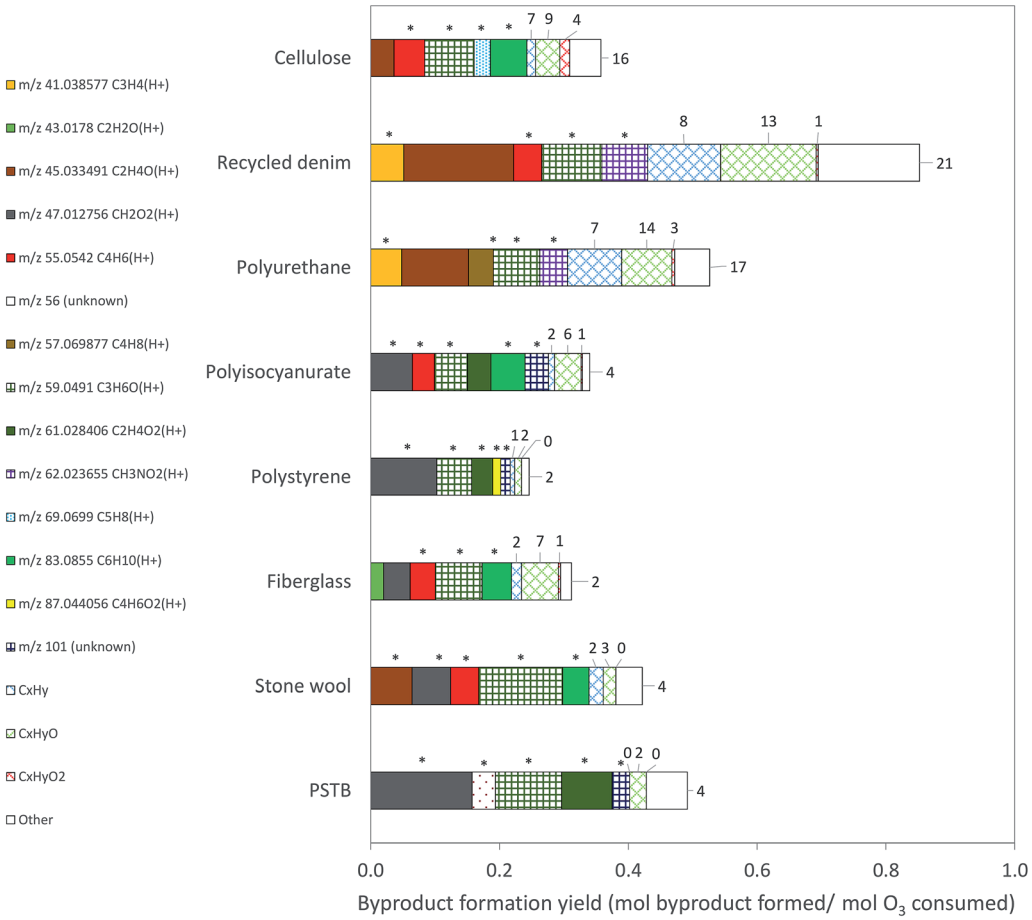

Fig. 5 Summary of byproduct formation yields for each tested material. Note that the data labels on the C_xH_y, C_xH_yO, $C_xH_yO_2$, and other categories refer to the number of unique, statistically significantly elevated compounds identified. Asterisks indicate compounds that were elevated in the presence of ozone and unique from those compounds observed in the primary emissions tests for that material. PSTB = polystyrene with thermal backing.

indoor fluid dynamics models with studies of emissions and transformation.

Detailed tables showing mass accuracy, putative chemical ID, and additional notes for compounds contributing significantly to the byproduct yield can be found in the ESI in Table S5.† Buhr *et al.*[58] showed that most aldehydes will lose a molecule of water leading to a main fragment at *m*/*z* (MH^+ – 18). Therefore, we attribute the peak at *m*/*z* 83 to a fragment of hexanal with a loss of a molecule of water (mass measured = 83.0804), consistent with the presence of a peak at *m*/*z* 101 possibly corresponding to the protonated parent compound. For the same reason, we also attribute the peak at *m*/*z* 55 to a fragment of butanal (MH^+ – 18) (exact mass = 55.054227, measured mass = 55.0454), confirmed by the presence of a peak at *m*/*z* 73 corresponding to protonated parent compound (exact mass = 73.06534, measured mass = 73.0411). However, this assignment should be taken with caution, as fragmentation of hexanal can lead to a signal at *m*/*z* 55, which may also be true of heptanal (Buhr *et al.*, 2002).[58] The presence of heptanal was also confirmed by the presence of a peak at *m*/*z* 97, which corresponds to a loss of water from the parent compound as well. Aldehyde fragments were found in cellulose, polyisocyanurate, fiberglass and stone wool insulation as well as recycled denim insulation, although the hexanal fragment (*m*/*z* 83) was not among statistically significant compounds for recycled denim.

Further limitations include the potential for presence of the structural isomers, such as propanal and acetone as oxygenated byproducts from reaction of the materials with O_3. Mass signals at *m*/*z* 59 were present for all materials. Only recycled denim and polyurethane contained significant signals at *m*/*z* 41, although at higher levels than would be expected due to fragmentation from a propanal parent at *m*/*z* 59. Thus, we conclude that for recycled denim and polyurethane, both acetone and propanal are likely present in the sampled air. Given the precedence for O_3–building material interactions to result in the formation of carbonyl compounds and acetone,[66] this finding is expected. The PTR-TOF-MS method does not enable the separation of these structural isomers, and so assignment of these compounds to signals in a matrix possibly containing both compounds is challenging.

Interestingly, cellulose appears to have a different secondary emission profile and yield from that of recycled denim although they had similar magnitude and composition of primary emissions. This is most likely due to differences in material or

surface-bound chemical composition of the two materials, leading to different heterogeneous chemistry that yields distinct oxygenated products. The largest byproduct yield for cellulose corresponds mainly to aldehyde fragments (m/z = 55, 69 and 83), acetone, and more widely to un-attributed mono- or di-oxygenated compounds.

Heterogeneous reactions of recycled denim and polyurethane with O_3 led to high formation yields for acetaldehyde (with contributions of acetaldehyde–water cluster at $m/z = 63.05$ according to Herbig *et al.*[67]), acetone, and, more generally, mono- and di-oxygenated compounds (~0.85 and ~0.53 mol mol^{-1} consumed for denim and polyurethane, respectively), making them the highest emitters of byproducts in the presence of O_3. Recycled denim and polyurethane had similar yield profiles. A peak at m/z 41 likely corresponds to a propanal fragment, pentanal fragment, and/or alcohol fragment according to Wyche *et al.*[68] (exact mass = 41.038577, measured mass = 41.0358). This peak was observed only for denim and polyurethane with a yield of 0.05 mol mol^{-1} for both materials and could be related to the oxidation of polyols present in polyurethane (polyols react in excess with isocyanates to make polyurethane and can still be present in the final polymer and give aldehydes that react with O_3 and could lead to carboxylic acid in presence of water). A peak at m/z 62 was found as a byproduct only in those two materials with relatively high yields (0.07 and 0.04 mol mol^{-1} for denim and polyurethane, respectively). We attributed this peak to the protonated carbamic acid (CH_3NO_2) due to its alignment with the exact mass (exact mass = 62.023655, measured mass = 62.0266). The formation of those compounds with only those two materials in the presence of O_3 might be explained by the presence of polyurethane in denim, which could explain the similar composition in VOCs primary emission and byproducts formation.

Formic acid (exact mass = 47.012756, measured mass = 47.0128) was common and one of the most elevated yields among five of the eight materials (present in fiberglass, stone wool, polyisocyanurate, polystyrene, and PSTB). Yield values ranged from 0.04 to 0.16 mol mol^{-1}. Polyisocyanurate, fiberglass, and stone wool had a similar profile of byproduct formation yield, with aldehyde fragments (for a total of 0.08, 0.09, and 0.08 mol mol^{-1}, respectively), formic acid (0.06, 0.04, and 0.06 mol mol^{-1}, respectively), and acetone (0.05, 0.07, and 0.13 mol mol^{-1}, respectively), with stone wool presenting a relatively high yield of acetaldehyde (0.06 mol mol^{-1}). Polystyrene and PSTB had a very similar profile, with higher yields for formic acid, acetone, and acetic acid with PSTB.

When considering both the removal of O_3 and the resulting byproduct formation yield, there exists a range of behaviors. In general, O_3 reactivity does not appear to be predictive of byproduct formation yield. Both cellulose and fiberglass have shown relatively high O_3 sink strengths compared to the other materials tested in this study, but their secondary TVOC formation rate is lower than other insulation materials. A potential reason for this is the cellulose and fiberglass surface compounds may be structured to allow for a catalytic decomposition pathway for O_3, resulting in the production of CO_2 and O_2. Recycled denim and polyurethane appear to have the opposite behavior. Lower deposition velocities were found for these two materials as compared to cellulose, but a higher formation yield was detected. Due to the fact that they have similar primary emission profiles as cellulose, the difference is most likely due to differences in surface morphology and the composition of these materials.

3.4 Limitations and future work

The work presented here represents, to our knowledge, a substantial expansion of the ozone reactivity and primary and secondary emission behavior of building insulation materials. However, there exist important sources of uncertainty in this investigation that compel future studies of this important class of building material. First, while we selected eight materials to span a range of commonly used insulation materials, there exist other types of wall enclosure products that should be tested. In addition, there are multiple manufacturers of any given type of insulation material, and variation in VOC emissions and ozone chemistry of a material type for any given manufacturer is also possible. Future work could investigate variability among similar products across different manufacturers as well as within-manufacturer variability (*e.g.*, subsampling across a single lot of material as well as acquiring samples from a single manufacturer with different manufacture dates).

The scope of this study was to investigate the VOC emissions and ozone reactivity of common building insulation materials, as manufactured. Future work would also be well-served by conducting additional characterization of materials to quantitatively capture differences in material chemical composition and morphology. These data would advance understanding of the drivers of observed differences in emission and reactivity behavior across materials. Primary emissions were measured over a period of 55 minutes, ideally, emissions would be measured over a longer time period to ensure full desorption of compounds that may have adsorbed to the material from other sources (*e.g.*, air in storage warehouse or in sample storage bag air). We attempted to minimize this source of error by keeping materials in their manufactured bags and limiting the amount of time the samples were exposed to laboratory air. Finally, while ionization *via* PTR-TOF-MS is, in theory, "soft", fragmentation of aldehydes is known phenomena that complicates the calculation of emission rates of this class of compounds. Furthermore, the PTR-TOF-MS is not a universal detector, future studies should inter-compare emission rates estimated with PTR-TOF-MS complemented by, and in comparison with, other analytical methods such as TD-GC-MS and HPLC-UV.

4 Conclusions

This study investigated the primary emissions, ozone (O_3) reactivity, and O_3 reaction byproduct emissions from eight commonly used building insulation materials. Results demonstrate that cellulose insulation was the largest emitter of primary VOCs, followed by recycled denim. Polystyrene, fiberglass, and stone wool had relatively low primary VOC emissions,

and polystyrene with thermal backing actually served as a sink for some VOCs. The O_3 reaction probability of these materials ranged more than an order of magnitude, and total reaction byproduct yields ranged from ~0.25 to ~0.85 moles of byproduct formed per mole of O_3 consumed. A number of secondary VOCs resulting from O_3 reactions were logically deduced (and varied by material), but further analysis should be done to clearly identify the secondary byproducts formed due to oxidation of insulation. To our knowledge, this study provides the first characterization of the aforementioned parameters for a range of common insulation materials. The data presented herein could serve as the basis for informing quantitative comparisons of trade-offs between different enclosure insulation materials, *e.g.*, consideration of thermal resistance in conjunction with material emissions, O_3 removal, and byproduct formation. These data can also inform building enclosure transport modelling efforts, which we recommend be improved upon in future work to incorporate the ability to predict the impacts of oxidation chemistry in building enclosures on both primary and secondary pollutant fluxes into the space.

Conflicts of interest

There are no conflicts to declare.

Acknowledgements

ETG was supported by start-up funds from the Portland State University College of Engineering. This material is based in part upon work supported by the National Science Foundation under Grant No. 1560383. BS was partially supported by an ASHRAE New Investigator Award.

References

1 J. M. Logue, T. E. McKone, M. H. Sherman and B. C. Singer, *Indoor Air*, 2011, **21**, 92–109.
2 C. J. Weschler, *Indoor Air*, 2000, **10**, 269–288.
3 M. L. Bell, A. McDermott, S. L. Zeger, J. M. Samet and F. Dominici, *J. Am. Med. Assoc.*, 2004, **292**, 2372–2378.
4 M. Jerrett, R. T. Burnett, C. A. Pope, K. Ito, G. Thurston, D. Krewski, Y. Shi, E. Calle and M. Thun, *N. Engl. J. Med.*, 2009, **360**, 1085–1095.
5 J. I. Levy, S. M. Chemerynski and J. A. Sarnat, *Epidemiology*, 2005, **16**, 458–468.
6 J. F. Gent, E. W. Triche, T. R. Holford, K. Belanger, M. B. Bracken, W. S. Beckett and B. P. Leaderer, *J. Am. Med. Assoc.*, 2003, **290**, 1859–1867.
7 J. L. Peel, M. Klein, W. D. Flanders, J. A. Mulholland, G. Freed and P. E. Tolbert, *Environ. Health Perspect.*, 2011, **119**, 1321–1327.
8 N. Fann, A. D. Lamson, S. C. Anenberg, K. Wesson, D. Risley and B. J. Hubbell, *Risk Anal.*, 2012, **32**, 81–95.
9 D. E. Hun, M. C. Jackson and S. S. Shrestha, *Optimization of Ventilation Energy Demands and Indoor Air Quality in the ZEBRAlliance Homes*, Oak Ridge National Laboratory, Oak Ridge, TN, 2013.
10 C. Hachem, P. Fazio, J. Rao, K. Bartlett and Y. P. Chaubey, *Build. Environ.*, 2009, **44**, 1691–1698.
11 H. Li, M. Yang, J. S. Zhang and M. Salonvaara, *ASHRAE Trans.*, 2005, **111**, 210–217.
12 W. R. Chan, W. W. Nazaroff, P. N. Price, M. D. Sohn and A. J. Gadgil, *Atmos. Environ.*, 2005, **39**, 3445–3455.
13 M. Ji, D. S. Cohan and M. L. Bell, *Environ. Res. Lett.*, 2011, **6**, 024006.
14 M. Yan, Z. Liu, X. Liu, H. Duan and T. Li, *Chemosphere*, 2013, **93**, 899–905.
15 D.-L. Liu and W. W. Nazaroff, *Atmos. Environ.*, 2001, **35**, 4451–4462.
16 C. J. Weschler, *Environ. Health Perspect.*, 2006, **114**, 1489–1496.
17 M. S. Waring, *Indoor Air*, 2014, **24**, 376–389.
18 C. Chen, B. Zhao and C. J. Weschler, *Environ. Health Perspect.*, 2012, **120**, 235–240.
19 I. S. Walker, M. H. Sherman and W. W. Nazaroff, *Ozone Reductions Using Residential Building Envelopes*, California Energy Commission, PIER Energy-Related Environmental Research Program, 2010.
20 I. S. Walker and M. H. Sherman, *Build. Environ.*, 2013, **59**, 456–465.
21 B. Stephens, E. T. Gall and J. A. Siegel, *Environ. Sci. Technol.*, 2012, **46**, 929–936.
22 H. Zhao and B. Stephens, *Indoor Air*, 2016, **26**, 571–581.
23 C. J. Weschler, *Atmos. Environ.*, 2004, **38**, 5715–5716.
24 C. J. Weschler, *Indoor Air*, 2004, **14**(7), 184–194.
25 G. Morrison, *Curr. Sustainable/Renewable Energy Rep.*, 2015, **2**, 33–40.
26 C. J. Weschler, *Indoor Air*, 2011, **21**, 205–218.
27 E. T. Gall, R. L. Corsi and J. A. Siegel, *Environ. Sci. Technol.*, 2014, **48**, 3682–3690.
28 E. T. Gall and D. Rim, *Build. Environ.*, 2018, **138**, 89–97.
29 S. P. Lamble, R. L. Corsi and G. C. Morrison, *Atmos. Environ.*, 2011, **45**, 6965–6972.
30 A. Vlasenko, J. G. Slowik, J. W. Bottenheim, P. C. Brickell, R. Y.-W. Chang, A. M. Macdonald, N. C. Shantz, S. J. Sjostedt, H. A. Wiebe, W. R. Leaitch and J. P. D. Abbatt, *J. Geophys. Res.: Atmos.*, 2009, **114**, D21305.
31 S. Inomata, H. Tanimoto, Y. Fujitani, K. Sekimoto, K. Sato, A. Fushimi, H. Yamada, S. Hori, Y. Kumazawa, A. Shimono and T. Hikida, *Atmos. Environ.*, 2013, **73**, 195–203.
32 R. Holzinger, A. Kasper-Giebl, M. Staudinger, G. Schauer and T. Röckmann, *Atmos. Chem. Phys.*, 2010, **10**, 10111–10128.
33 J. Zhao and R. Zhang, *Atmos. Environ.*, 2004, **38**, 2177–2185.
34 C. Sarkar, V. Sinha, V. Kumar, M. Rupakheti, A. Panday, K. S. Mahata, D. Rupakheti, B. Kathayat and M. G. Lawrence, *Atmos. Chem. Phys.*, 2016, **16**, 3979–4003.
35 B. K. Coleman, M. M. Lunden, H. Destaillats and W. W. Nazaroff, *Atmos. Environ.*, 2008, **42**, 8234–8245.
36 G. C. Morrison and W. W. Nazaroff, *Environ. Sci. Technol.*, 2002, **36**, 2185–2192.
37 O. A. Abbass, D. J. Sailor and E. T. Gall, *Atmos. Environ.*, 2017, **148**, 42–48.
38 J. A. Cano-Ruiz, D. Kong, R. B. Balas and W. W. Nazaroff, *Atmos. Environ.*, 1993, **27**, 2039–2050.

39 A. Kumari and K. Khurana, *Regenerated Cellulose-Based Denim Fabric for Tropical Regions*, https://www.hindawi.com/journals/jtex/2016/4614168/, accessed November 26, 2018.
40 N. Hayeck, B. Temime-Roussel, S. Gligorovski, A. Mizzi, R. Gemayel, S. Tlili, P. Maillot, N. Pic, T. Vitrani, I. Poulet and H. Wortham, *Int. J. Mass Spectrom.*, 2015, **392**, 102–110.
41 M. C. Area and H. Cheradame, *BioResources*, 2011, **6**, 5307–5337.
42 H. Kraessig, *J. Polym. Sci., Part C: Polym. Lett.*, 1987, **25**, 87–88.
43 M. Strlič, I. K. Cigić, J. Kolar, G. De Bruin and B. Pihlar, *Sensors*, 2007, **7**, 3136–3145.
44 M. Risholm-Sundman, M. Lundgren, E. Vestin and P. Herder, *Holz Roh- Werkst.*, 1998, **56**, 125–129.
45 R. C. Pettersen, in *The Chemistry of Solid Wood*, American Chemical Society, 1984, vol. 207, pp. 57–126.
46 S. Tohmura, A. Ishikawa, K. Miyamoto and A. Inoue, *J. Wood Sci.*, 2012, **58**, 57–63.
47 Videojet Technologies, Inc., L. Zhu, G. Deng and F. Xiao, *US Pat.*, US8110031B2, 2012.
48 T. Łojewski, T. Sawoszczuk, J. M. Łagan, K. Zięba, A. Barański and J. Łojewska, *Appl. Phys. A: Mater. Sci. Process.*, 2010, **100**, 873–884.
49 T. M. Ruuskanen, M. Müller, R. Schnitzhofer, T. Karl, M. Graus, I. Bamberger, L. Hörtnagl, F. Brilli, G. Wohlfahrt and A. Hansel, *Atmos. Chem. Phys.*, 2011, **11**, 611–625.
50 J. L. Rivera-Armenta, T. Heinze and A. M. Mendoza-Martínez, *Eur. Polym. J.*, 2004, **40**, 2803–2812.
51 D. G. Poppendieck, M. Gong, L. E. Lawson and S. J. Emmerich, No. *NIST Interagency/Internal Report (NISTIR)-8131*, 2016.
52 GTZ Proklima, *Natural Foam Blowing Agents*, Federal Ministry for Economic Cooperation and Development (BMZ), Environment and Sustainable Use of Natural Resources Division, 2012.
53 D. G. Poppendieck, M. Gong and S. J. Emmerich, *Tech. Note NIST TN*, 1921.
54 E. A. Bruns, J. G. Slowik, I. E. Haddad, D. Kilic, F. Klein, J. Dommen, B. Temime-Roussel, N. Marchand, U. Baltensperger and A. S. H. Prévôt, *Atmos. Chem. Phys.*, 2017, **17**, 705–720.
55 T. Maihom, E. Schuhfried, M. Probst, J. Limtrakul, T. D. Märk and F. Biasioli, *J. Phys. Chem. A*, 2013, **117**, 5149–5160.
56 E. Dunne, I. E. Galbally, S. Lawson and A. Patti, *Int. J. Mass Spectrom.*, 2012, **319–320**, 40–47.
57 BASF Corp., T. Narayan, G. G. Ramlow and P. T. Kan, *US Pat.* and Trademark Office, US06225934, 1981.
58 K. Buhr, S. van Ruth and C. Delahunty, *Int. J. Mass Spectrom.*, 2002, **221**, 1–7.
59 C. Yu and D. Crump, *Build. Environ.*, 1998, **33**, 357–374.
60 Y.-H. Cheng, C.-C. Lin and S.-C. Hsu, *Build. Environ.*, 2015, **87**, 274–282.
61 I. S. Walker and D. J. Wilson, *HVACR Res.*, 1998, **4**, 119–139.
62 Z. Gao and J. S. Zhang, *HVACR Res.*, 2012, **18**, 160–168.
63 D. Lai, P. Karava and Q. Chen, *Build. Environ.*, 2015, **93**, 112–118.
64 E. T. Gall, J. A. Siegel and R. L. Corsi, *Environ. Sci. Technol.*, 2015, **49**, 4398–4406.
65 G. C. Morrison and W. W. Nazaroff, *Environ. Sci. Technol.*, 2000, **34**, 4963–4968.
66 E. Gall, E. Darling, J. A. Siegel, G. C. Morrison and R. L. Corsi, *Atmos. Environ.*, 2013, **77**, 910–918.
67 J. Herbig, T. Titzmann, J. Beauchamp, I. Kohl and A. Hansel, *J. Breath Res.*, 2008, **2**, 037008.
68 K. P. Wyche, R. S. Blake, A. M. Ellis, P. S. Monks, T. Brauers, R. Koppmann and E. C. Apel, *Atmos. Chem. Phys.*, 2007, **7**, 609–620.